

An Empirical Correction for Moderate Multiple Scattering in Super-Heterodyne Light Scattering

**Denis Botin^{1,*}, Ludmilla Marota Mapa^{1,2}, Holger Schweinfurth¹, Bastian Sieber¹,
Christopher Wittenberg¹, and Thomas Palberg¹**

¹Institut für Physik, Johannes Gutenberg Universität, D-55099 Mainz, Germany

²Institute of Chemical Engineering, Federal University of Itajubá

Frequency domain super-heterodyne laser light scattering is utilized to determine flow and diffusion in charged sphere suspensions showing moderate multiple scattering. We introduce an empirical correction to subtract the multiple scattering background and isolate the singly scattered light. We demonstrate the excellent feasibility of this simple approach for turbid suspensions as long as the transmittance $T \geq 0.4$. To characterize the diffusive dynamics the low angle integral signal in the absence of any external field is analysed. We show that depending on the choice of suitable samples, we can measure either the self or the collective diffusion coefficient. Moreover, we are able to study the particle concentration of the DC electro-kinetic properties of weakly ordered charged particles in low salt aqueous suspension over an extended concentration regime. Somewhat counter-intuitively, we observe that the mobility first increases with increasing particle concentration, then shows a plateau and finally decreases again.

PACS: if needed

corresponding author: Denis Botin dbotin@uni-mainz.de

INTRODUCTION

Moderate multiple scattering (MS) is a nuisance in Laser light scattering. Sophisticated techniques have been developed and employed to study the dynamics of turbid colloidal suspensions [1]. At very large turbidities and small optical path lengths, diffusive wave spectroscopy (DWS) may be employed [2]. In the regime of low multiple scattering, index matching is regularly employed [3, 4, 5], but it is not easily applicable in water based systems. Further, optical path lengths may be shortened by utilizing fibre optics [6]. In addition, cross correlation schemes pioneered by Phillies in the early eighties [7] and further developed to two color or 2D cross correlation schemes are employed [8]. This way the methods and theory developed for dynamic light scattering in the time domain could be used also in turbid samples [9]. Alternatively, in frequency domain special mode selective heterodyne instrumentation was developed and applied to Brillouin scattering [10, 11, 12]. Mode selection and cross correlation however afford complex instrumentation and data evaluation schemes. Being interested in flow measurements and employing Laser Doppler velocimetry, we were intended to minimize the extra complexity. Doppler velocimetry is a well-established frequency domain technique used to study the flow properties of colloidal dispersions. A typical application is the determination of the electro-phoretic mobility $\mu_e = \mathbf{v}_e / \mathbf{E}$ which can be interpreted in view of the particle zeta potential [13, 14]. Here \mathbf{v}_e is the drift velocity of a particle in the applied electric field \mathbf{E} . Previous research has revealed two differing types of particle concentration dependence. In some studies the mobility was found to first increase, but then to saturate with increasing particle number density, n [15, 16, 17]. The transition to a concentration independent mobility seems to correlate to the onset of inter-particle ordering, i.e. to conditions of strongly overlapping electric double layers. Moreover, increase and saturation have been observed in systems of quite different salt concentrations $10^{-6} \text{ mol/l} \leq c_s \leq 10^{-2} \text{ mol/l}$ [18]. The observed behaviour stays theoretically unexplained. However, in other studies we observed the mobility to start with a plateau, but then to decrease [19, 20]. In the latter case, the onset of the decrease coincides with the onset of counter ion dominance, i.e. when the counter-ions of the charged particles start to dominate the small ion population [21]. This is reproduced in computer simulations [20] and theoretically understood in terms of the electrolyte concentration dependence of the zeta potential [22]. Together, the experimental observations seem to suggest the existence of a broad maximum in the density dependent mobility. However, so far, no single study has reported all the three different dependencies for

a given particle species, which would resolve the apparent contrast between different observations.

The reason for this lack of data is mainly technical. Practically all data showing the ascent were measured on particles with large scattering cross section, i.e. particles with large radii, a , and/or refractive index contrast. This yields a good signal-to-noise-ratio even at low particle number density, n , but leads to problems with MS contributions at large n . Conversely, small particles are causing less multiple scattering and can be investigated up to large n and even in the crystalline region of the phase diagram [23]. However, at low n the signal becomes vanishingly small.

The present paper therefore suggests a facile empirical correction applicable to moderate multiple scattering, which considerably extends the accessible range of particle number densities in LDV and provides a low budget alternative for conventional DLS in turbid samples. It is based on the pronounced separation of time scales for decorrelation for multiply and singly scattered light. This allows subtracting the MS contribution to the Doppler spectra after a simple fit procedure and thus isolating the singly scattered spectral contribution. We demonstrate the scope and limits of this approach by three examples. First, we determine the collective diffusion coefficient, $D_C(q)$ in a weakly ordered sample of low polydispersity latex spheres with and without the presence of shear flows. This allows to quantify the amount of Taylor dispersion in flow direction as a function of overall flow. In the limit of zero shear and infinite dilution the standard Stokes-Einstein-Sutherland diffusion coefficient, D_0 , is recovered. Second, we measure the self-diffusion coefficient, D_S in two crystallizing samples of an optically inhomogeneous co-polymer latex sample at two different volume fractions. We can follow the decrease of this quantity during solidification and annealing of grain boundaries and observe the expected decrease of D_S with increased interaction strength. Most importantly, however, we utilize our approach to obtain MS free Doppler spectra of suspensions in electro-kinetic flow even at large turbidity. We evaluate the isolated single scattering spectra for electro-kinetic velocities and observe a broad maximum for μ_e at moderate particle number densities. Albeit still preliminary, our study thus indicates a reconciliation of previously divergent interpretation of the concentration dependence of the electro-phoretic mobility.

In what follows we first outline the experimental procedure, which has been slightly modified as compared to previous approaches using super-heterodyne LDV [24, 25, 26, 17, 27]. In the experimental section we introduce the two samples and their preparation, describe the actual

LDV measurements and present representative Doppler spectra with and without applied electric field. We then shortly recall the principle of single scattering integral, low-angle, super-heterodyne LDV with special focus on the specific advantages of the present LDV instrument for density dependent measurements. We show that the evaluation scheme based on single scattering utterly fails in describing the multiple scattering contaminated spectra. After that, we introduce our empirical correction scheme based on the separation of time scales of de-correlation by multiple scattering and particle motion. In the results section we show how to obtain different diffusivities in the absence or presence of flow as well as electro-kinetic velocities induced by electric fields. In the latter case, we also characterize the MS contribution to the LDV spectra in some detail and determine the concentration dependence of the electro-phoretic mobility over an extended range. In the discussion section we focus on the performance and limits of this scheme. We find our procedure to perform remarkably well even for a transmittance of 0.4. We close with an outlook on future applications.

EXPERIMENTAL METHODS AND EVALUATION SCHEME

Integral, low-angle, super-heterodyne LDV

Our home-built Laser Doppler Velocimetry (LDV) instrument combines the reference beam integral measurement of [28] (allowing to measure the complete flow-profile in a single measurement) with super-heterodyning [29, 30] (allowing to separate the heterodyne part of the power spectrum from the homodyne part and low frequency noise). The present machine is a modification of the previously described setup [27], now also allowing a continuous variation of the scattering angle. The essential part of this instrument is sketched in Fig. 1.

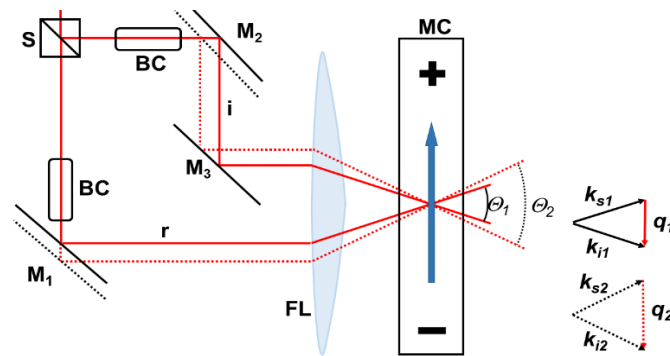


Fig. 1: Sketch of the experimental scattering geometry with two alternative optical paths, r and i, indicated. To the right, we show the resulting difference in the scattering vector \mathbf{q} . For details see text. The direction of particle motion is indicated by the blue arrow.

The beam of a He-Ne laser of circular frequency $\omega_0 \approx 10^{15}$ Hz is split into two beams, a reference beam (r) and an illuminating beam (i), using a beam splitter (S). Each beam passes through a Bragg-cell (BC, Model 3080-125, Crystal Technology Inc., USA with a frequency shifter DFD 80, APE GmbH, Germany) and is frequency-shifted by the circular frequencies $\omega_i/2\pi = 80.002$ MHz and $\omega_r/2\pi = 80.000$ MHz, with the larger frequency shift realized for the illuminating beam (upper beam in Fig. 1). This results in a positive relative Bragg-shift, $\Delta\omega_B = \omega_i - \omega_r$ in the circular frequency corresponding to $\Delta f_B = \Delta\omega_B / 2\pi = (2000 \pm 5)$ Hz. The beams are redirected into the sample cell (MC) by a set of mirrors (M_1 to M_3) and a lens (FL). There they cross in the suspension under an angle $\Theta = (5 - 28)^\circ$. (Note that in Fig. 1, we show the beam propagation in air.) An improvement as compared to previous set-ups is that here Θ can be continuously varied simply by shifting the mechanically coupled mirrors M_1 and M_2 . In Fig. 1, a downward shift to the dotted positions increases the scattering vector \mathbf{q} .

On the detection side (not shown), a polarizer, to assure V/V detection, and a set of apertures, to define the observed sample volume, are arranged on the reference beam optical axis. For our so-called integral measurements, light, scattered off the particles in the complete illuminated part of the sample, is received within the acceptance angle of a grin lens defining the scattering vector \mathbf{q} . The lens is mounted at the inlet of an optical fibre leading to a photomultiplier used to record the intensity. The scattering vector $\mathbf{q} = \mathbf{k}_i - \mathbf{k}_s$, where \mathbf{k}_i and \mathbf{k}_s are the wave vectors of the illuminating and scattered beams, is parallel to the applied field direction (c.f., Fig. 1). In the present sign convention, \mathbf{q} is proportional to the momentum transfer from the photon to the scattering particle. Its modulus is given by $q = (4\pi\nu_S / \lambda_0) \sin(\Theta_S/2) = (4\pi / \lambda) \sin(\Theta/2)$, where ν_S is the index of refraction of the solvent and Θ_S is the beam crossing angle in the suspension. We note, that light scattered by a particle j moving with a velocity \mathbf{v}_j is Doppler-shifted by the circular frequency $\omega_D = -\mathbf{q} \cdot \mathbf{v}(x,y)$, where the velocity can be a function of the position. The frequency shift, ω_D , is positive, if the particle velocity shares an obtuse angle with the scattering vector, $\mathbf{q} = q \hat{\mathbf{z}}$, where $\hat{\mathbf{z}}$ is the unit vector in z -direction. Hence, a positive Doppler shift corresponds to particles moving towards the detector.

The reference beam is also directed into the fibre and is superimposed with the scattered light. It therefore acts as a local oscillator, and gives rise to beats in the observed intensity which are analysed by a Fast Fourier Transform analyser (Ono Sokki DS2000, Compumess, Germany) to yield the power spectrum as a function of frequency, $f = \omega / 2\pi$. To obtain a good signal to noise ratio typically some 200-2000 subsequent spectra are averaged. The power spectra are transferred to a computer, where the multiple scattering correction is applied and the corrected spectra are further evaluated for the electro-kinetic mobilities.

Single scattering super-heterodyne Doppler spectra

Non-interacting particles

While some progress has been made in the treatment of double scattering (e.g. [11, 31, 32]), the complexity of the theory for triple and higher-order scattering means that the theoretical approach has found little application in practice. We therefore correct our experimental signals for noise background and MS contributions and apply single scattering theory for their evaluation. The theoretical frame is based on earlier work on homo- and heterodyning techniques in dynamic light scattering [9, 33]. A theory of conventional heterodyne LDV using an integral reference beam set-up was outlined in [24]. Super heterodyne theory for integral measurements at low angles has been detailed in [27]. Further extensions to include de-correlation effects such as Taylor-dispersion arising in sheared solvents [34] and a rigorous treatment of electro-phoretic mobility polydispersity will be presented in a forthcoming paper [35]. Here, we only shortly summarize the main theoretical points for single scattering following [27].

Our experiment determines the power spectrum, $C_{shet}(\mathbf{q}, \omega)$, which is the time Fourier transformation of the mixed-field intensity autocorrelation function, $C_{shet}(\mathbf{q}, \tau)$, and given by:

$$C_{shet}(\mathbf{q}, \omega) = \frac{1}{\pi} \int_{-\infty}^{\infty} d\tau \cos(\omega\tau) C_{shet}(\mathbf{q}, \tau) \quad (1)$$

with circular frequency ω and correlation time τ . For a scattered light field of Gaussian statistics the latter quantity is given as:

$$C_{shet}(\mathbf{q}, \tau) = (I_r + \langle I_S(\mathbf{q}) \rangle)^2 + 2I_r \langle I_S(\mathbf{q}) \rangle \text{Re}[\hat{g}_E(\mathbf{q}, \tau) \exp(-i\omega_B \tau)] + \langle I_S(\mathbf{q}) \rangle^2 |\hat{g}_E(\mathbf{q}, \tau)|^2 \quad (2).$$

Here, I_r is the reference beam intensity, $\langle I_S(\mathbf{q}) \rangle$ is the time-averaged scattered intensity, and $\hat{g}_E(\mathbf{q}, \tau) = g_E(\mathbf{q}, \tau) / \langle I_S(\mathbf{q}) \rangle$ is the normalized field autocorrelation function. For a suspension

of non-interacting, monodisperse particles of diffusion coefficient D and constant drift velocity \mathbf{v}_0 the power spectrum reads

$$\begin{aligned}
C_{shet}^0(\mathbf{q}, \omega) = & \left[I_r + \langle I_S^0(\mathbf{q}) \rangle \right]^2 \delta(\omega) \\
& + \frac{I_r \langle I_S^0(\mathbf{q}) \rangle}{\pi} \left[\frac{q^2 D}{(\omega + [\omega_B - \omega_D])^2 + (q^2 D)^2} + \frac{q^2 D}{(\omega - [\omega_B - \omega_D])^2 + (q^2 D)^2} \right] \\
& + \frac{\langle I_S^0(\mathbf{q}) \rangle^2}{\pi} \frac{2q^2 D}{\omega^2 + (2q^2 D)^2}
\end{aligned} \tag{3}$$

Here, the index 0 indicates these idealized conditions and $\omega_D = \mathbf{q} \cdot \mathbf{v}_0$ is the frequency of the Doppler shift. The spectrum contains three contributions: a trivial constant term centred at zero frequency, two super-heterodyne Lorentzians shifted away from the origin by both the Bragg frequency and the Doppler frequency, and the homodyne Lorentzian of double width which is independent of the particle drift motion and is again centred at the origin. Analysis of the super-heterodyne Lorentzians therefore allows determining both the electro-phoretic and diffusive particle motion.

In the absence of flow, $\omega_D = 0$. Then the super-heterodyne Lorentzians are centred at $\pm\omega_B$. Under the flow particles typically show a velocity distribution, $P(\mathbf{v})$. The Doppler spectra then display a corresponding distribution of Doppler frequencies, $P(\omega_D)$. This can be accounted for by a convolution integral:

$$C_{shet}(\mathbf{q}, \omega) = \int d\omega_D P(\omega_D) C_{shet}^0(\mathbf{q}, \omega) \tag{4}$$

Assuming that all particles have the same mobility, the velocity distribution in our electrokinetic experiment is determined only by the solvent flow profile. Our measurements are performed in a closed cell with negatively charged walls. Application of an electric field therefore leads to an electro-osmotic flow along the cell walls and a counter-propagating backflow of the incompressible solvent in the cell centre. In Fig. 2a, we sketch the resulting solvent flow profile $\mathbf{u}_S(x, y)$ for a cell of height $2h$ and depth $2d$ in units of the electro-osmotic velocity at the wall, $\mathbf{u}_{e0} = \mu_e \mathbf{E}$, where μ_{e0} is the electro-osmotic mobility. This profile was calculated according to [36] using the boundary condition of no net solvent flow. The particle velocity results as the sum of particle electro-phoretic velocity and solvent profile $\mathbf{v} = \mathbf{v}_e + \mathbf{u}_S(x, y, \mathbf{E})$. Here, $\mathbf{v}_e = \mu_e \mathbf{E}$ is the particle velocity relative to the solvent depending on

its electro-phoretic particle mobility μ_e and the electric field \mathbf{E} . Fig. 2a shows the lab coordinate system with x -, y -, and z -directions denoting the direction of the optical axis or cell depth direction, the cell height direction and the direction of particles moving along the field, respectively. The origin is taken to be at the cell centre. In our experiments we measure the velocity distribution at mid-plane cell height ($y = 0$). Under this conditions the particle flow profile, $\mathbf{v}(x, y = 0)$ can be analytically approximated as [37]:

$$\mathbf{v}(x, y = 0) = \mu_e \mathbf{E} + \mu_{eo} \mathbf{E} \left[1 - 3 \left(\frac{1 - \frac{x^2}{d^2}}{2 - \frac{384}{\pi^5 K}} \right) \right] \quad (5)$$

Here, $K = h/d$ is the ratio of cell height, h , to cell depth, d . The resulting mid-plane flow-profile is sketched in Fig. 5c for $K = 5$. It is parabola-like and the corresponding $P(v)$ is asymmetric with a pronounced maximum at the centre velocity [24].

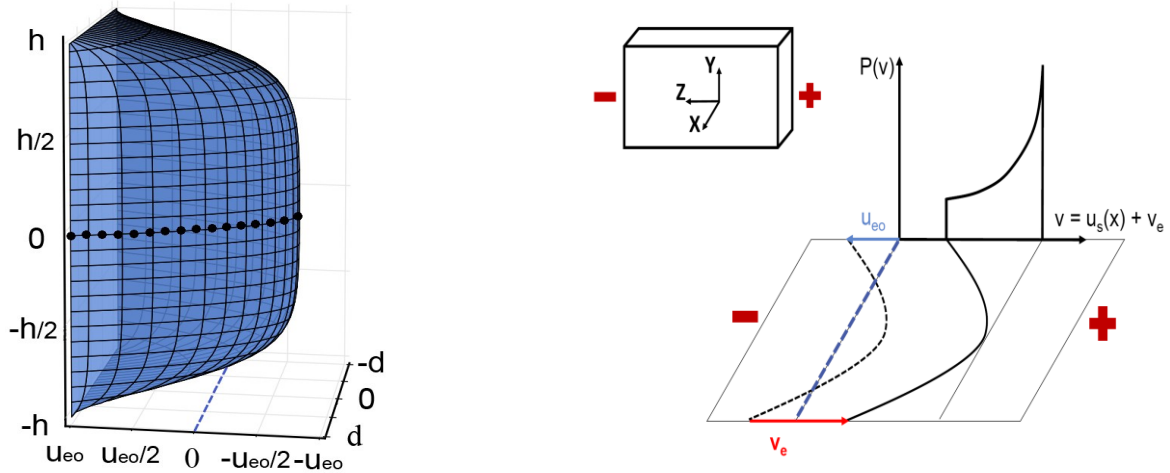


Fig. 2: Top: sketch of the closed measuring cell with coordinate system and electrodes are indicated. Thickness of the cell in x -direction is $2d$, height is $2h$, z -axis points in field direction. Left: Solvent velocity profile $\mathbf{u}_s(\mathbf{x}, \mathbf{y})$ inside a cell of $K = 5$ in units of the electro-osmotic solvent velocity at the wall $\mathbf{u}(x = |d|, y) = \mathbf{u}_{eo} = \mu_{eo} \mathbf{E}$, where μ_{eo} is the electro-osmotic mobility. Note the pronounced central backflow at $x \approx 0$ which is nearly independent of y . The black dotted line denotes the cell's mid-plane. Right: particle velocity distribution in the mid-cell x - z -plane at $y = h = 0$ for superimposing solvent flow and electro-phoretic motion. The blue dashed line denotes zero velocity. Electrode positions are indicated. Negatively charged colloids move to the right and display a negative velocity. Further, a negatively charged cell wall induces a negative solvent velocity in the center. Both effects superimpose and the resulting particle velocity distribution, $P(v)$ is rightward shifted away from the origin.

We note, that in Eqn. (3) only the super-heterodyne term is of interests and, moreover, this term is symmetric about the origin. In Fig. 4 and also the following, we therefore display the measured data only for positive frequencies centred about the positive Bragg shift frequency. Interestingly, this is already sufficient to infer the sign of the electro-kinetic velocities. A positive centre of mass frequency $\omega_0(E)$ corresponds to a negative velocity \mathbf{v}_P and hence a negative electro-phoretic mobility μ_e and a negative particle charge. A maximum at the high frequency side corresponds to a positive wall velocity \mathbf{u}_{eo} and hence to a negatively charged wall.

Interacting particles

The situation becomes somewhat more complex for interacting particles. Then $C_{shet}(\mathbf{q}, \tau)$ depends on the suspension structure through several effects. Most notably, structure may couple to flow properties resulting in inhomogeneous shear thinning or shear banding [38, 39], alteration of the particle flow profile due to local crystal cohesion [40, 41], and even time-dependent effects [42]. Such cases where Eqn. (5) is not applicable are not considered in the present experiments, However, they can be treated using systems with dominant incoherent scattering [27], where the electro-phoretic velocity is calculated according to $v_e = \langle \langle v_P \rangle_x \rangle_y$ as the y -average of the x -averaged velocities [42].

Upon the evolution of structure, coherently scattered and incoherently scattered contributions to the spectra will differ. To switch between domination of coherently and incoherently scattered light we utilize a low angle configuration and suitable particles. Moreover, in both cases we exploit that the intensity of light scattered coherently at low angles ($q \Rightarrow 0$) becomes very small due to the decreased isothermal compressibility of the suspension. This does, however, not alter any incoherent scattering contribution arising from optical polydispersity, which therefore becomes dominant at low q [43, 44]. Assuming a purely optical polydispersity arising from a size polydispersity of standard deviation s , the normalized field autocorrelation function can be written using the decoupling approximation as [27]:

$$g_E(\mathbf{q}, \tau) = \overline{I_0 n f^2(q)} S_M(\mathbf{q}, \tau) \approx \overline{I_0 n f^2(q)} \left[9s^2 G(q, \tau) + S(\mathbf{q}, \tau) \right] \quad (6)$$

Here $\overline{f^2(q)}$ is the average scattering cross section of the particles. $S_M(\mathbf{q}, \tau)$ is the so-called measurable dynamic structure factor, $S(\mathbf{q}, \tau)$ is the dynamic structure factor arising from coherent scattering and $G(q, \tau)$ is the self-intermediate scattering function. The amplitude of the latter for $\tau = 0$ is independent of the suspension structure and the chosen \mathbf{q} [44]. Note, that

Eqn. (6) describes the limiting case in the absence of any additional optical polydispersity, e. g. due to internal inhomogeneity of the particles. In that latter case, the weight of $G(\mathbf{q}, \tau)$ is further increased.

To measure self-diffusion or flow properties, we employ deionized suspensions of particles with optical polydispersity (e.g. co-polymer particles or partially crystalline particles). These yield signal shape and strength independent of any local system structure by exploiting the low angle dominance of incoherent scattering in strongly interacting suspensions [43, 44]. This has been previously utilized to measure electro kinetic properties of well-ordered colloidal fluids and crystals showing negligible MS [27]. The other limit of a vanishing incoherent contribution is obtained for suspensions of optically homogeneous particles of moderate polydispersity. To be specific, under the studied conditions $S(\mathbf{q}) \geq 0.8 \gg 0.007$. Hence, all Doppler spectra can be interpreted in terms of a velocity distribution, but from their diffusive broadening one either obtains $D = D_S$ or $D = D_C(\mathbf{q})$ depending on the choice of system.

Determination of diffusivities under flow may be further complicated by an effect termed Taylor dispersion [34], which accounts for the apparent increase of diffusion in a shear gradient. Furthermore, the spectral broadening may depend on field induced velocity fluctuations [10] or a polydispersity of the electro-phoretic mobility [45]. As a consequence of all these mechanisms a linear dependence of fitted D_{eff} on the field strength has frequently been observed [24]. Due to the lack of detailed knowledge about the ratio of different contributions under flow, no prediction for the field-dependent spectral broadening can be made. In any case the spectra can be fitted using an effective diffusion coefficient $D_{\text{eff}}(E)$, but only in the field free case, an interpretation in terms of a diffusion coefficient can be reliably attempted. The field free self-diffusion coefficient has been observed to decrease with increasing particle concentration and interaction strength [46]. Also the coherently measured diffusive decay of $S(\mathbf{q}, \tau)$ depends on the time and length scale considered [44]. The short time collective diffusion coefficient scales with $H(\mathbf{q})/S(\mathbf{q})$ (where $H(\mathbf{q})$ is the hydrodynamic function [32]) and thus increases with increasing particle concentration and interaction strength.

Sample selection and preparation

The sample for measurements of electro-kinetic properties and collective diffusion comprises of commercial polystyrene latexes stabilized by carboxylate surface groups (lab code PS310,

manufacturer batch #1421. IDC, Portland, USA). Their nominal diameter is 310 nm as given by the manufacturer. Their hydrodynamic radius $a_H = 167$ nm and polydispersity index $PI = 0.8$ were determined by dynamic light scattering measurements on dilute samples [47]. These particles show a low amount of incoherent scattering.

The particles employed for measurements of self-diffusion are a 35:65 W/W copolymer of Poly-n-Butylacrylamide (PnBA) and Polystyrene (PS), kindly provided by BASF, Ludwigshafen (Lab code PnBAPS118 manufacturer Batch No. 1234/2762/6379). Their nominal diameter of (117.6 ± 0.65) nm and nominal polydispersity index of $PI = 0.011$ were determined by the manufacturer utilizing dynamic light scattering. TEM analysis and form factor measurements using SAXS yield $PI \approx 0.06$. These particles show strong incoherent scattering.

Sample preparation used procedures described in detail elsewhere [48, 49, 50]. Precleaned stock suspensions were diluted with milli-Q grade water. Samples were loaded into a thermostatted peristaltic conditioning circuit. Circuit contains an ion exchange column filled with mixed bed ion exchange resin (Amberlite, Room&Haas, France), a reservoir to add water or further stock suspension, a conductivity experiment (electrodes LR325/01 and LR325/001; bridge LF340i, WTW, Germany) and a cell for static light scattering, all connected via Teflon® tubings. The suspension is peristaltically cycled and the drop of conductivity with progressing deionization is noted. With pure water, the set-up suffices to reach conductivities below 60 nScm^{-1} after some ten to twenty minutes. For the larger final conductivity reached with particles added, we estimate the residual ion concentration to be on the order of $c \leq 1 \times 10^{-6} \text{ mol/l}$. The suspension static structure factor was measured in a home-built multi-purpose light scattering instrument [51] and evaluated for the particle number density n . The number density dependence of the conductivity of PS310 is shown in Fig. 3. From the slope we derive an effective number of freely moving H^+ - counter-ions, $Z_{\text{eff}} = 5260 \pm 100$ using the model of independent ion conductivity [49, 52]. Within charge renormalization theory, this corresponds to saturation value of $A = 8.01 k_B T$ [53]. The effective charge for PnBAPS118 is $Z_{\text{eff}} = 647 \pm 18$.

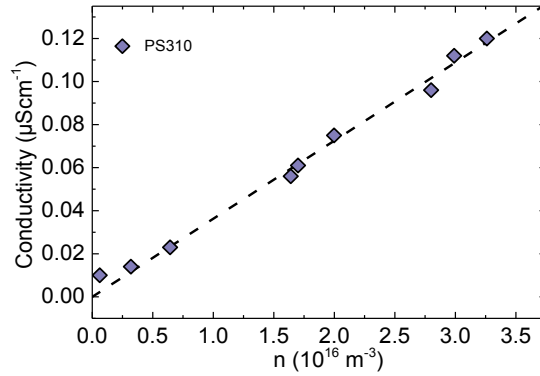


Fig. 3: Number density dependence of the low frequency AC conductivity of deionized PS310. Dashed line shows a fit of the theoretical expectation for this quantity within the model of independent ion conductivity [49, 52]

For PnBAPS118, the preparation circuit was then disconnected from the static light scattering cell and connected to the electro-phoretic cell. This way we could easily alter the particle concentration but maintain a thorough deionization under conductometric control. After conditioning, the measuring chamber is isolated from the remaining circuit by electromagnetic valves to avoid residual flows and minimize contamination with airborne CO₂. For number densities above $n = 0.2 \mu\text{m}^{-3}$, PnBAPS118 then readily crystallizes in a body centred cubic structure.

For PS310, suspensions of different n were first conditioned as described above. Then small amounts of the suspension were pipetted to rectangular quartz cells of $2d = 1 \text{ mm}$ and $2d = 2 \text{ mm}$ optical path length (Hellma, Germany) and transferred to a home built turbidity measurement working at 633 nm. The transmittance or relative transmitted intensity, $T = I/I_0$, was recorded as a function of n , where I_0 refers to the cells filled with milli-Q grade water. Fig. 4 shows the result. We note that conductivity measurements were not feasible in this set-up. Therefore, samples were exposed to ambient air to obtain CO₂-saturated conditions. The residual ion concentration in this case was estimated to be $c_s \leq 5 \times 10^6 \text{ mol l}^{-1}$.

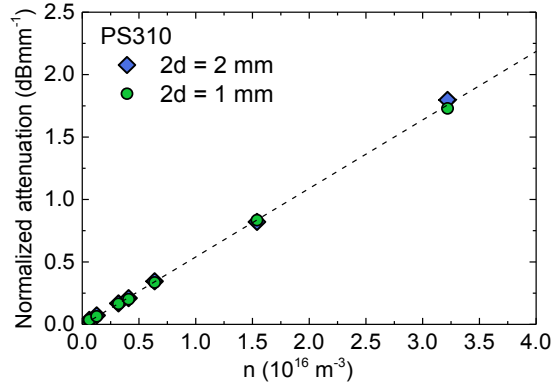


Fig. 4: Attenuation of transmitted intensity normalized to the cell thickness $2d$ as a function of the number density n . Results of the two measurements coincide. A fit of Eqn. (7) returns an attenuation cross-section of $\sigma_{633} = 0.13 \pm 0.1 \mu\text{m}^2$.

The transmitted intensity for deionized or low salt suspensions is known to obey the Lambert-Beer-law in both the fluid and crystalline state [54]:

$$2dn\sigma_{633} = -\ln\left(\frac{I}{I_0}\right) \quad (7)$$

From fits of Eqn. (7) to the data, we obtained an attenuation cross-section of $\sigma_{633} = 0.13 \pm 0.1 \mu\text{m}^2$.

To ensure identical optical properties in both turbidity experiments and LDV, PS310 have to be conditioned the same way. The large background salinity has yet another advantage for the present LDV study. At the low volume fractions utilized, the suspensions will not develop a crystalline nor even pronounced fluid order. Rather it will show a pronounced forward scattering. This is ideally suited to demonstrate the scope of the here introduced MS-correction scheme. For each concentration, a second amount of sample was therefore filled into the electro-phoresis cell (Rank, Bottisham, Cambridge, UK) used in the SH-LDV experiment. The u-shaped electro-phoretic cell has its electrode chambers separated from the actual optical section of rectangular cross section of $(10 \times 1) \text{ mm}^2$ and width $l = 40 \text{ mm}$. The effective platinum electrode distance is $L \approx 80 \text{ mm}$. It was determined precisely before each measurement series from calibration with an electrolyte dilution series.

During the measurements, the electrode chambers are sealed. No field is applied in diffusion measurements. In electro-kinetic measurements alternating square-wave fields of strength up to $E_{MAX} = U/L = 15 \text{ V/cm}$ were applied. To avoid accumulation of particles at the electrodes and to further ensure fully developed stationary flows [25], field switching frequencies $f_{AC} =$

(0.02 – 0.1) Hz were used. Measurement intervals were restricted to the one field direction. Each starting after the full development of electro-osmotic flow profile and ending shortly before the field reversal. Generally, we recorded and averaged 250 full time-frame power spectra for each field strength. For diffusion measurements in PnBAPS118, we typically averaged over 1000-2000 time frames. For rapidly crystallizing samples of that species, many repeated shear-melting - recrystallization cycles were performed to obtain the temporal evolution of the diffusive properties.

Typical spectra

Typical examples of averaged power spectra for PS310 and $E = 0$ at $n = 1.64 \times 10^{16} \text{ m}^{-3}$ as well as for $E = 4.3 \text{ Vcm}^{-1}$ and increasing n are shown in Fig. 5 and 6, respectively. Raw spectra for PnBAPS118 appear to be similar to Fig. 5. If there is no field applied, only a single broad spectral feature centred at 2 kHz is present. It varies in strength and broadness for changing n .

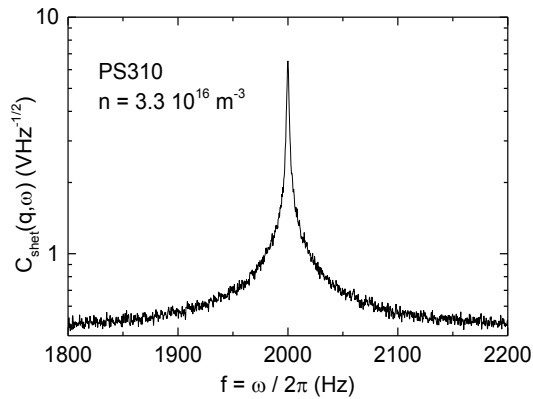


Fig. 5: Power spectrum of PS310 at $n = 1.64 \times 10^{16} \text{ m}^{-3}$ and $2d = 2 \text{ mm}$, recorded in the multiple scattering regime without applied electric field. A single broad spectral feature is visible which is centred at the Bragg shift frequency, $f_B = 2000 \text{ Hz}$.

This is different in the case of applied field, where we can clearly discriminate different types of spectral contributions due to their different spectral shape. At very low n , the characteristic shape of the electro-phoretic signal [21] is barely visible in the background noise. With extensive further averaging, an acceptable signal may be obtained for $n \geq 8 \times 10^{14} \text{ m}^{-3}$. Excellent noise free signals are obtained for $2 \times 10^{15} \text{ m}^{-3} \leq n \leq 8 \times 10^{16}$. A background signal becomes discernible for $n \geq 1 \times 10^{16} \text{ m}^{-3}$ which increases with increasing n until it dominates the power spectrum for $n > 10^{17} \text{ m}^{-3}$. This signal contribution is attributed to multiple

scattering. It appears to be symmetric with a maximum close to the Bragg frequency, $f_{MS} \approx \Delta f_B = 2000\text{Hz}$. At $n = 1 \times 10^{17} \text{ m}^{-3}$ the sample transmission $T < 0.05$, and even the reference beam is strongly attenuated. The spectrum becomes noisier and the signal to background ratio decreases significantly. As the regime of strong multiple scattering is approached, the LDV signal disappears, and the spectrum becomes finally dominated by electric power grid harmonics.

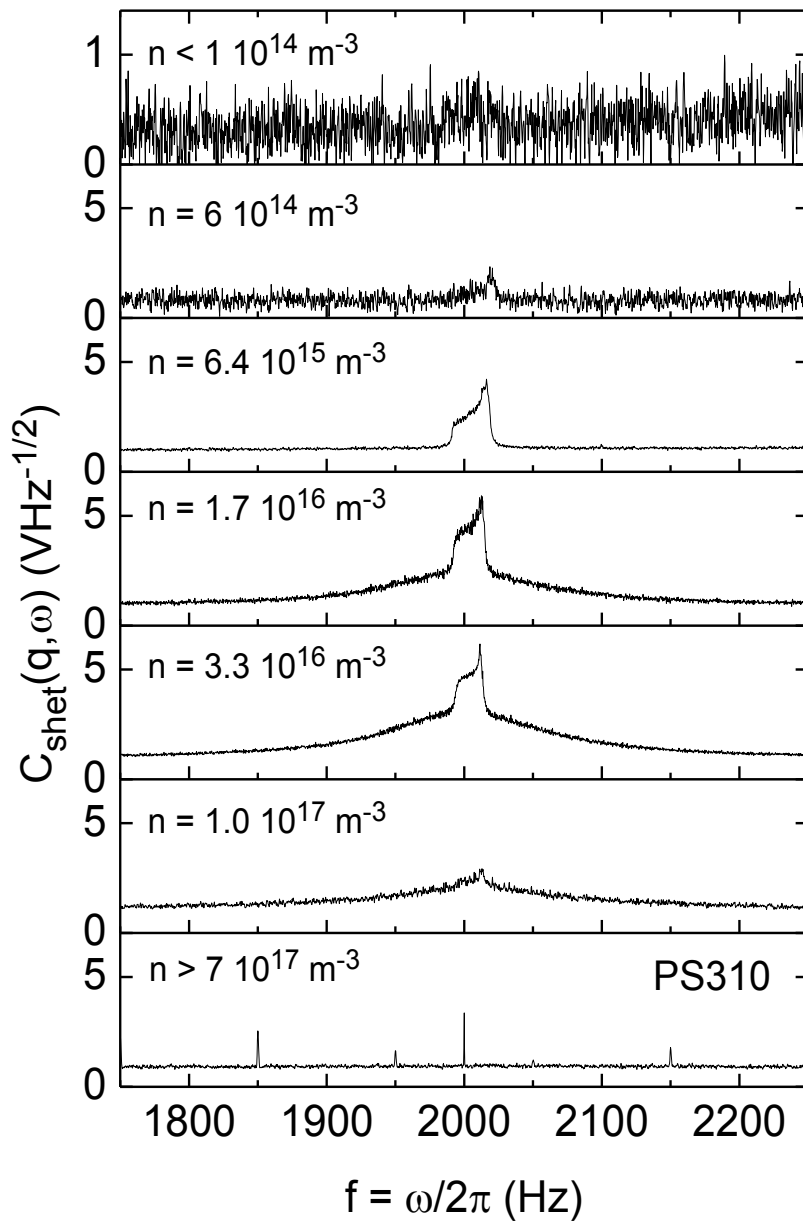


Fig. 6: Examples of power spectra obtained at a field strength of $E = 4.3 \text{ Vcm}^{-1}$ for deionized suspensions of PS310 at different particle number densities as indicated. Background noise,

electro-phoretic spectrum and multiple scattering background each show distinct spectral shapes. With increasing n , the ratio of contributions changes. For PS310, the actual Doppler-spectra emerge from the background noise for $n > 5 \times 10^{14} \text{ m}^{-3}$ and vanish in the multiple scattering background for $n > 1 \times 10^{17} \text{ m}^{-3}$. Both contributions are centred close to the Bragg shift frequency, $f_B = 2000 \text{ Hz}$. In the limiting case of optically dense samples, transparency is lost and the signal disappears completely leaving only the contributions of electronic noise. Note that the signal is clearly visible for concentrations covering more than two orders of magnitude in n .

As shown in Fig. 6, measurements of relatively turbid samples yield spectra composed of a background resulting from noise, a Doppler spectrum and a symmetric MS background. Their relative contribution varies with n . We average the noise background at frequencies far off the other spectral features and subtract it from the data. We then perform a least square fit of a theoretical expression for $C_{\text{shet}}(q, \omega)$ derived from a combination of Eqns. (1) to (5) with the cell geometry, the field strength and the particle number density as input. Over one order of magnitude in n , i. e. for spectra in the range of $8 \times 10^{14} \text{ m}^{-3} \leq n \leq 8 \times 10^{15} \text{ m}^{-3}$, we obtained excellent fits with u_{eo} , v and D_{eff} as independent fit parameters. Attempts to fit the spectrum at larger n , lead to unsatisfactory results due to the contribution by multiple scattering (MS). This is illustrated in Fig. 7 for a spectrum recorded for PS310 at deionized conditions, $E = 5.3 \text{ Vcm}^{-1}$, $n = 1.64 \times 10^{16} \text{ m}^{-3}$ and $2d = 2 \text{ mm}$. Our theory can predict the spectral shape only for single scattering. We therefore tried a simple but effective empirical correction scheme for the evaluation of the MS contaminated data.

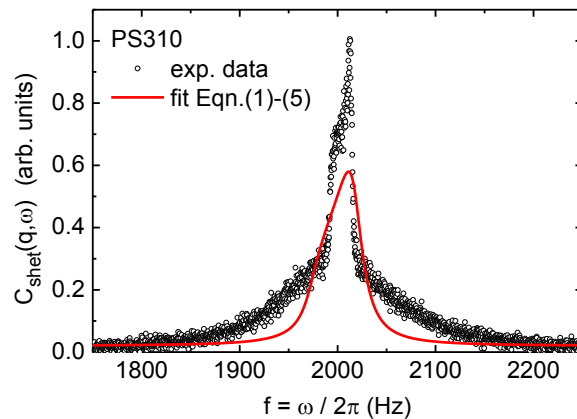


Fig. 7: Low angle integral super-heterodyne spectrum of PS310 recorded at $E = 5.3 \text{ Vcm}^{-1}$ with $n = 1.64 \times 10^{16} \text{ m}^{-3}$, $2d = 2 \text{ mm}$ and $K = 5$. Data are normalized to unity at the maximum.

Solid red line is the best least square fit obtainable with the theoretical expressions described above.

We first address the field free case in which the broad spectral feature centred at 2 kHz remains. However, according to Eqn. (3) it is superimposed only by a simple Lorentzian, which is not easily discriminated by eye (c.f. Fig. 5). We therefore assume a superposition of different statistically independent spectral contributions and fit the data with the empirical expression:

$$C_{shet}(\mathbf{q}, \omega) = A + A' \int dv P(v) C_{shet}^0(\mathbf{q}, \omega, v, D_{eff}) + \frac{B}{2\pi} \frac{w}{(\omega_B - \omega)^2 + w^2} \quad (8)$$

Here, A is a constant describing the frequency independent noise background, A' is the amplitude of the Doppler spectrum depending on the ratio of coherently to incoherently scattered light from single scattering events, B is the area of the MS contribution, also modelled as Lorentzian centred at ω_B and of full width at half height, w. We note that the choice of this functional form is not primarily based on a physical assumption. It was chosen due to its superior performance as compared to a Gaussian and other bell shaped curves. For $E = 0$, only Eqn. (1) to (3) are necessary to calculate the single scattering super-heterodyne spectrum and $P(v)$ is a δ -function at $v = 0$. An example fit to data obtained in the field free case is shown in Fig. 8, with the inset magnifying the central region of the spectrum.

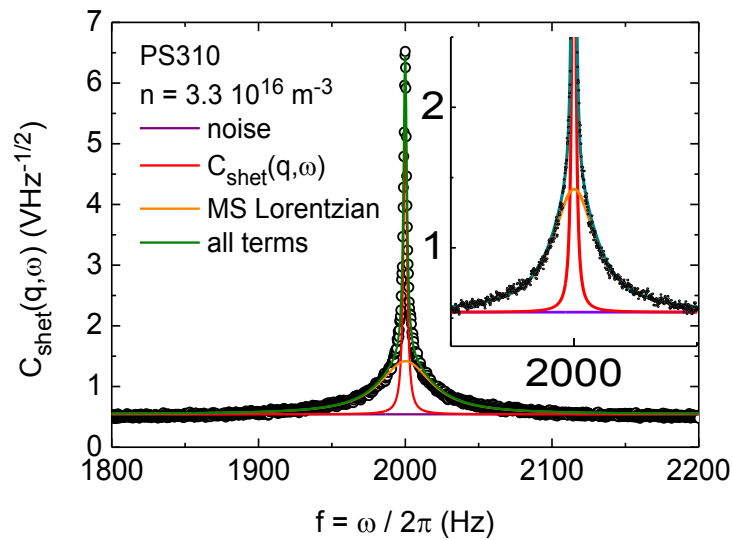
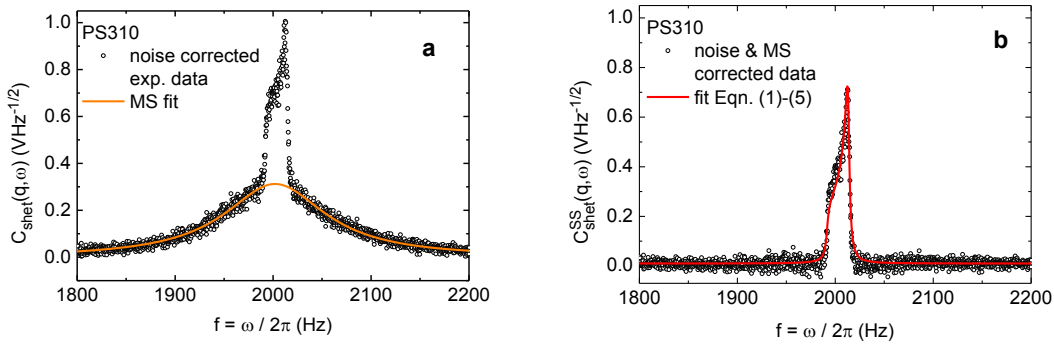


Fig. 8: Power spectrum of PS310 at $n = 1.64 \times 10^{16} \text{ m}^{-3}$ and $2d = 2 \text{ mm}$, recorded in the multiple scattering regime without applied electric field (black circles). Also shown is the fit of Eqn. (8) (solid green line) which is the superposition of a constant background noise (solid

violet line), the Lorentzian single scattering super-heterodyne power spectrum (solid red line) and a second Lorentzian describing the multiple scattering contribution (solid orange line). An excellent fit is obtained, showing the applicability of our empirical correction scheme.

Next, we applied this correction scheme to data obtained for PS310 at finite field strengths. Fig. 9a and b exemplify this for the data of Fig. 7. First, in Fig. 9a the MS Lorentzian (orange solid curve) is fitted to the wings of the spectral feature that remained, after the noise background was fitted far off the spectral features and subtracted. After subtraction of the MS contribution the remaining experimental data are fitted in Fig. 9b by a theoretical expression based on Eqn. (1) to (5). An excellent fit is obtained in Fig. 9b using the fit parameters: $v_e = 37.4 \mu\text{ms}^{-1}$, $u_{e0} = 64.1 \mu\text{ms}^{-1}$, $D_{\text{eff}} = 4.49 \times 10^{-12} \text{ m}^2\text{s}^{-1}$.

Finally, we turn to PnBAPS118. Here, the MS contribution, the background noise and the signal were much smaller than for PS310 even at large number densities. Still, MS correction was both necessary and unproblematic. In some cases, however, the single scattering spectrum was so weak that it became comparable to a residual 2kHz feature. The latter originates from the interference of the reference with of parasitic stray light from the illumination beam and is not considered in Eqn. (3). We therefore applied a minute plug flow ($v \approx 1 \mu\text{m/s}$) to shift the centre of the heterodyne Lorentz by a few Hz and separate the signal from the artefact. This is shown in Fig 9c. We then fitted the spectrum by our expression for the single scattering integral super-heterodyne power spectrum based on Eqns. (1) to (5) plus an additional narrow Lorentzian for the 2 kHz-peak. For the example shown in Fig. 9c, an excellent fit is obtained returning $D_S = 1.43 \times 10^{-13} \text{ m}^2\text{s}^{-1}$.



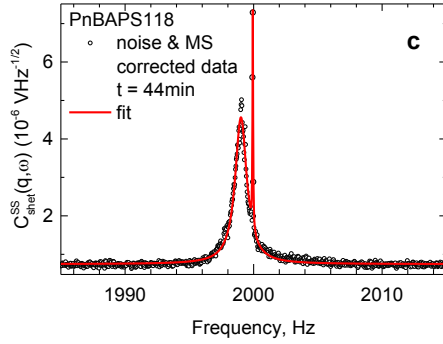


Fig. 9: Data fitting. a) data of Fig. 6 after subtraction of a constant noise background term with the MS Lorentzian (orange solid line) fitted to the wings of the spectral feature. b) Isolated single scattering power spectrum obtained by subtraction the fitted MS contribution from the data in a). The single scattering data are fitted with a theoretical expression for the single scattering integral super-heterodyne power spectrum based on Eqns. (1) to (5). An excellent fit is obtained using $v_e = 37.4 \mu\text{ms}^{-1}$, $u_{eo} = 64.1 \mu\text{ms}^{-1}$, $D_{\text{eff}} = 4.49 \times 10^{-12} \text{ m}^2\text{s}^{-1}$. c) Isolated single scattering power spectrum of poly-crystalline PnBAPS118 after MS and noise correction. Note the low signal intensity. This spectrum was recorded 44 min after stop of shear over a time interval of 5 min. A minute flow was applied to separate the spectral contributions (for details see text). Data are fitted with a theoretical expression for the single scattering integral super-heterodyne power spectrum based on Eqns. (1) to (5) plus an additional Lorentzian for the 2kHz peak. An excellent fit is obtained returning $D_S = 1.43 \times 10^{-13} \text{ m}^2\text{s}^{-1}$.

RESULTS

The above tested procedures were applied to all systematic measurements for both zero and finite field strength. This gives access to the characteristics of the MS contribution for PS310, the zero flow diffusion coefficients of PnBAPS118 during and shortly after crystallization and, most importantly, the electro-kinetic properties of PS310 and their dependence on particle number density.

The multiple scattering contribution

The results for the number density dependence of the MS contribution at zero field are summarized in Fig 10. We note that with increasing number density, both the MS intensity reaching the detector and the spectral width of the MS background increase approximately linearly. In Fig. 10a, we show the dependence of the integrated spectral intensity of the

isolated MS Lorentzian as a function of n . By extrapolating the data linearly to zero integrated intensity, we find that for PS310, MS starts a threshold of $n_{\text{thres}} = (0.4 \pm 0.05) \times 10^{16} \text{ m}^{-3}$. In Fig. 9b, we show the dependence of the full width at half height of the isolated MS Lorentzian as a function of n for the case of $E=0$. By extrapolating the data linearly to zero width, we find that for PS310, MS starts a threshold of $n_{\text{thres}} = (0.3 \pm 0.1) \times 10^{16} \text{ m}^{-3}$. Both values are consistent with each other within experimental uncertainty. We note that this threshold number density corresponds to 10% extinction for the case of weakly ordering PS310. For PnBAPS118 a qualitatively similar behaviour was observed at overall lower integrated intensities.

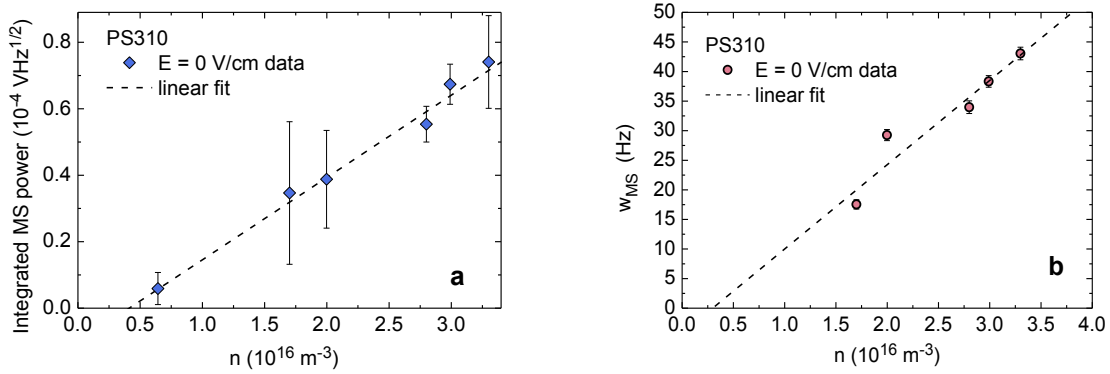


Fig. 10: a) Linear fit of the n -dependent integrated spectral power of the isolated MS Lorentzian returning a MS threshold of $n_{\text{thres}} = (0.4 \pm 0.05) \times 10^{16} \text{ m}^{-3}$. b) Linear fit of the n -dependent full width at half height of the MS Lorentzian returning a MS threshold of $n_{\text{thres}} = (0.3 \pm 0.1) \times 10^{16} \text{ m}^{-3}$.

Next, we investigate the field strength dependence of the MS contribution. No significant dependence of the integrated spectral power of the MS contribution on the applied field strength was observed. In Fig. 11a and b, we show the dependence of the spectral width of the MS contribution on the applied field strength for three representative number densities. In Fig. 10a representative data are plotted in a linear fashion. All three curves nearly coincide, and one observes an approximately linear increase with E from an offset at $E = 0 \text{ Vcm}^{-1}$. For larger field strengths, a larger scatter in the data can be seen which, however, does not depend in a systematic way on n . The extra broadening thus mainly depends on the field strength. This is illustrated in Fig. 11b, where we have subtracted the zero field width and show the data in a double-logarithmic plot.

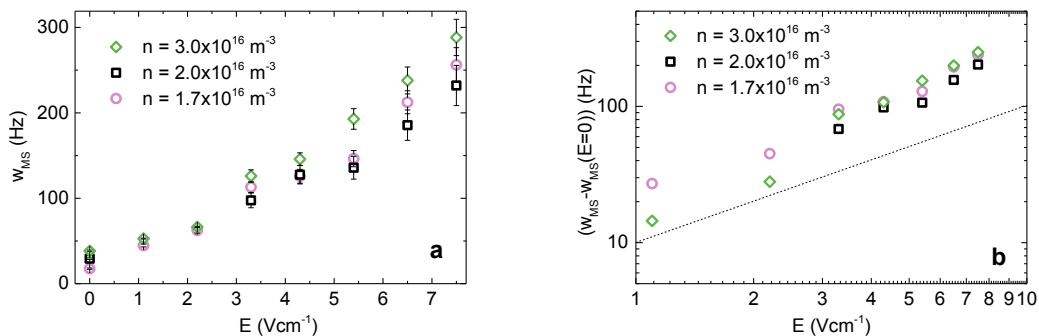


Fig. 11: a) Dependence of the spectral width of the MS contribution on the applied field strength. We observe a roughly linear increase from an offset at $E = 0 \text{ Vcm}^{-1}$. This is seen even more clearly in b), where we plot the data with the zero field width subtracted in a double-logarithmic fashion. The dotted line of slope 1 is a guide to the eye.

The MS contribution therefore contains some information on the particle motion. Recalling Eqn. (4), the measurable particle velocity, $\mathbf{v} = \mathbf{v}_E + \mathbf{u}_S$, depends on the solvent velocity as well as on the particle electro-phoretic velocity relative to the solvent. While the spatially averaged solvent velocity is zero, the spread of solvent velocities and the particle electro-phoretic velocity increase linearly with the field strength. In Fig. 12, we therefore check for a possible correlation between the central frequency of the MS Lorentzian and the central frequency of the single scattering power spectrum. At first sight, the values of the former appear to be at roughly half the values of the latter. Further, and in particular for low n , data show a clear trend to increase approximately linear with increasing field strength. However, the dependence is much less pronounced at the larger n and an offset appears. Therefore, we cannot find any simple correlation of the central frequency of the MS Lorentzian to any of the electro-kinetic velocities involved. Apart from stating that the average particle velocity has a negative sign, we have to refrain from any further evaluation of the MS contribution for electro-kinetic quantities.

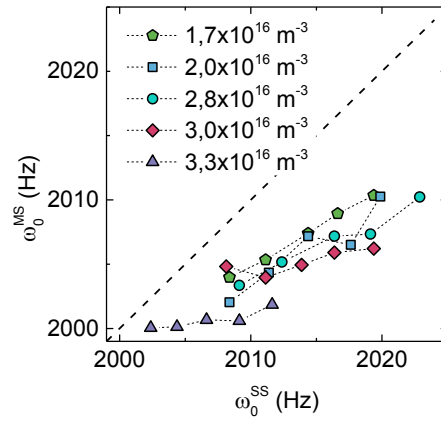


Fig 12: Centres of mass of the MS contribution plotted versus the centres of mass of the single scattering contribution for different particle densities as indicated. Within each n -series the field strengths increase from left to right covering a range of $(1-5) \text{ Vcm}^{-1}$. The dotted line indicates a direct proportionality. Below, data assemble on straight lines for each n . The field strength dependence of the MS central frequency appears to be considerably weaker than that of the single scattering central frequency. Moreover, the dependence seems to become weaker for increased n and an offset appears.

The single scattering power spectrum

Diffusion

The collective diffusion coefficients obtained for PS310 in the field free case are shown in Fig. 13a as triangles. They were obtained from fitting Eqn. (1) to (3), using $\nu = 0$, to the noise and MS corrected spectra for $n \geq 1.6 \times 10^{16} \text{ m}^{-3}$ measured at zero field. The collective diffusion coefficient shows a slow increase with increasing n . An extrapolation to $n = 0$ yields $D_C(n=0) = (5 \pm 2.5) \times 10^{-13} \text{ m}^2 \text{ s}^{-1}$. For comparison, the Stokes-Einstein-Sutherland self-diffusion coefficient for PS310 is $D_0 = k_B T / 6\pi\eta a_H = 6.6 \times 10^{-13} \text{ m}^2 \text{ s}^{-1}$, where we used a viscosity of water of 1 mPas and $a_H = 167 \text{ nm}$ as determined by standard DLS.

For comparison, we also show the field dependence of the effective diffusion coefficient of PS310 measured at three different n and various field strengths. The effective diffusivity increases with increasing field strength. The same behaviour also occurs at other n . Following [27], we extrapolate the field dependent effective diffusion coefficient to $E = 0$. Fig. 13a shows the extrapolated zero field effective diffusion coefficients as a function of number density (circles). One observes an approximately linear increase with increasing n starting

from a value of $D_{\text{eff}}(n=0) = (8\pm 3)\times 10^{-13} \text{ m}^2\text{s}^{-1}$, which is again close to D_0 . At any finite concentration, the extrapolated zero field effective diffusion coefficients are appreciably larger than the collective diffusion coefficients obtained in the field free case

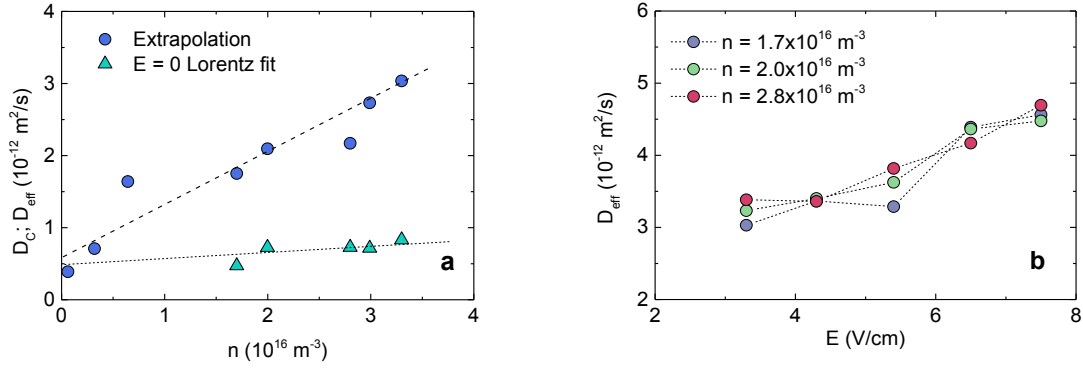


Fig. 13: Diffusive properties of PS310 without and with applied field. a) Comparison of the collective diffusion coefficient (triangles) measured at zero field to the extrapolated zero field effective diffusion coefficients (circles) obtained by extrapolation of the field dependent effective diffusion coefficients measured at finite field. Note the significantly different n -dependencies. In both cases, extrapolation to $n = 0$ yields nearly the same value close to the theoretically expected value at infinite dilution of $D_0 = 6.6 \times 10^{-13} \text{ m}^2\text{s}^{-1}$. b) Field dependence of the effective diffusion coefficient derived from the field dependent spectral broadening of the noise and MS corrected data for PS310 at various indicated number densities. In each case one observes a linear increase with increasing field.

PnBAPS118 shows a completely different behaviour. At low n both coherent and incoherent scattering contributions are present. Dominant incoherent scattering is obtained for $n > 0.2 \times 10^{18} \text{ m}^{-3}$ where the deionized sample starts crystallizing. This allowed studying the self-diffusion coefficient during and shortly after the crystallization. In general, the zero field diffusion coefficient decreases with increasing n and with time. For the early measurements we averaged over many repeated shear-melting – re-crystallization cycles. This ensured an acceptable statistical error for D_s . The systematic uncertainties are believed to be still larger because in each run only 10 to 50 crystals are found within the scattering volume. Therefore, we here present only the observed trends and refrain from a quantitative interpretation. Fig. 14 shows the results of two crystallization/coarsening experiments at $n = 0.5 \times 10^{18} \text{ m}^{-3}$ and $n = 2.5 \times 10^{18} \text{ m}^{-3}$. At all times, diffusion is way below D_0 and notably slower in the case of the more concentrated and hence more strongly interacting sample. This is in line with theoretical

expectations for self-diffusion in the fluid and the undercooled melt [46, 55] as well as with other experimental investigations on solidifying samples [56].

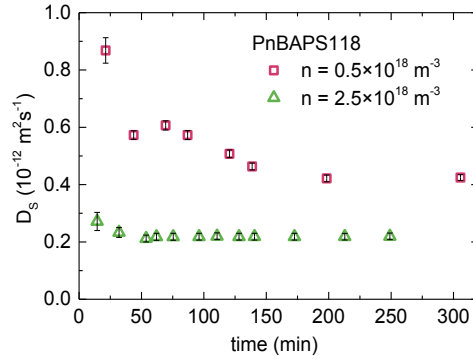


Fig. 14: Development of the self-diffusion coefficient for two crystallization/coarsening experiments at $n = 0.5 \times 10^{18} \text{ m}^{-3}$ and $n = 2.5 \times 10^{18} \text{ m}^{-3}$. Error bars denote the statistical uncertainty; the systematic errors are expected to be larger as the measuring volume contains only 10-50 crystals.

Electro-kinetics

We next apply our scheme to the complete set of measurements performed on PS310 in the presence of electric fields to obtain the n -dependence of their electro-phoretic mobility. Five different field strengths were applied for each number density. For each parameter set, 250 spectra were averaged. Using our empirical correction scheme, we obtained high quality, MS free single scattering super-heterodyne power spectra. All spectra could be fitted with high confidence to obtain the electro-kinetic mobilities of particles and cell wall. This is illustrated in Fig. 15a, where we show the isolated single scattering super-heterodyne power spectrum of PS310 at $n = 3.3 \times 10^{16} \text{ m}^{-3}$. For this sample, the transmittance was merely 0.4. As the field strength is increased, the spectra stretch and their centres of mass shift to larger frequencies. This is excellently described by the corresponding fits, which were performed using a combination of Eqns. (1) to (5). They return the electro-phoretic velocity of the particles, \mathbf{v}_e , the electro-osmotic solvent velocity at the cell walls, \mathbf{u}_{eo} , and an effective diffusion coefficient, D_{eff} . The obtained field-dependent velocities are displayed in Fig. 15b. They are on the order of several tens of μm per second and show a strictly linear dependence on the applied field strength.

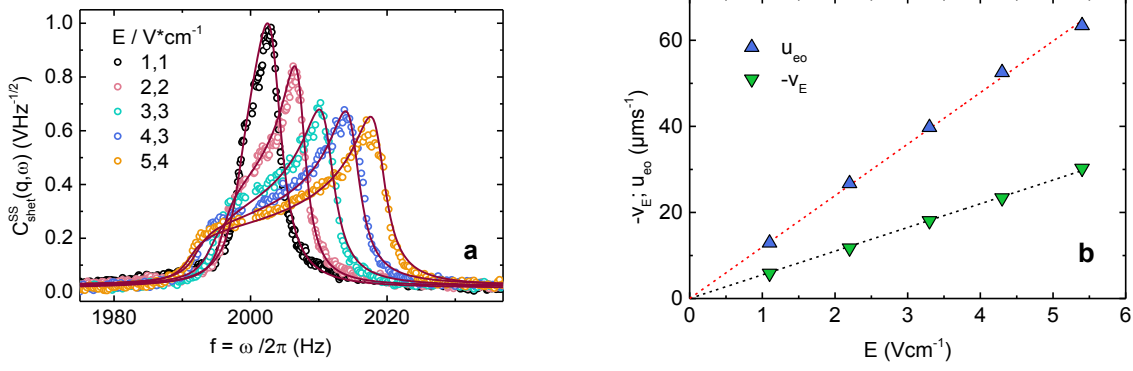


Fig. 15: a) Isolated single scattering Doppler spectra for PS310 at $n = 3.3 \cdot 10^{16} \text{ m}^{-3}$ and various field strengths as indicated. Solid lines are fits based on Eqn. (1) to (5). b) Electro-osmotic velocity at the cell walls, u_{eo} , and electro-phoretic particle velocity, v_p , as a function of field strength, as obtained from the fits in a). The field dependence of both velocities is strictly linear. From the slope, we obtain the electro-phoretic and electro-osmotic mobilities as $\mu_e = -5.4 \pm 0.1 \cdot 10^{-8} \text{ m}^2\text{V}^{-1}\text{s}^{-1}$ and $u_{eo} = 1.2 \pm 0.2 \cdot 10^{-7} \text{ m}^2\text{V}^{-1}\text{s}^{-1}$.

Under this condition of linear electro-kinetic response, the respective slopes equal the electro-phoretic particle mobility, μ_{ep} , and the electro-osmotic mobility along the cell wall, μ_{eo} . Following the IUPAC convention, both mobilities are converted to reduced units to eliminate the dependencies on solvent viscosity, η , and solvent dielectric permittivity $\epsilon_0\epsilon_r$ as well as on temperature, T [13]:

$$\mu^{red} = \mu \frac{3\eta e}{2\epsilon_0\epsilon_r k_B T} \quad (9)$$

Here e is the elementary charge and $k_B T$ denotes the thermal energy. The results for μ_e^{red} are plotted in Fig. 16 as a function of particle number density. The reduced mobility first increases, then displays a plateau at a value of about 5.8, then sharply decreases again. The corresponding reduced electro-osmotic mobilities are systematically larger but show a less pronounced density dependence.

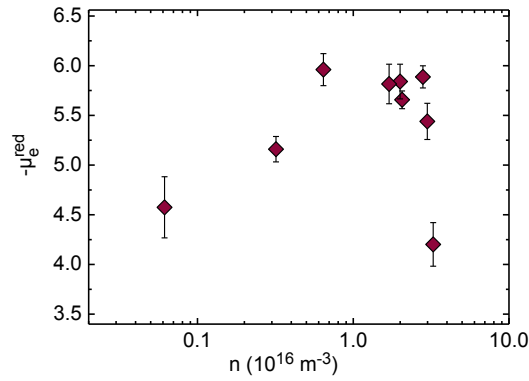


Fig. 16: Reduced electro-phoretic mobilities μ_e^{red} for PS310, measured under deionized conditions as a function of the particle number density n over roughly two orders of magnitude in n . Data for $n > 1 \times 10^{16} \text{ m}^{-3}$ were obtained performing both a correction for noise and for the MS scattering contribution. Note that the mobilities are negative for the negatively charged particle species. With increasing particle concentration, the electro-phoretic mobility shows an increase followed by a broad maximum and a steep decrease.

DISCUSSION

In our experiments, a MS contribution to the raw spectra became discernible for transmittances $T < 0.9$. We introduced and successfully tested an empirical correction scheme to isolate the single scattering contributions. This scheme could be reliably applied down to transmittances $T > 0.4$, while the signal finally disappeared at $T < 0.15$. For the electro-kinetic measurements on PS310 this corresponded to an extension of the accessible volume fraction range by nearly one order of magnitude. A similar extension is also anticipated in other situations, where weakly ordered suspensions are under investigation. These may include rheological measurements as well as measurements of active particles. While suspensions of strongly interacting samples are fairly transparent at low angles, this is not the case at larger angles and in particular around the maxima in the static structure factor. Even though the present experiments were performed only at a single angle without exploiting the possibility of q -dependent measurements, our method appears to be very flexible and our correction scheme should be readily applicable also many other cases without the need for instrumentally demanding cross correlation or mode selection schemes.

It relies on the presence of well-defined relaxation times and a clear separation of time scales between the de-correlation of scattered light due to MS and due to the physical processes

within the samples. It is well known from the dynamic light scattering measurements in the time domain, that in the case of multiple scattering, the autocorrelation function shows a pronounced initial decay on short time scales on the order of μs or faster. This de-correlation occurs due to the random phase shift introduced by the next scattering event involving a particle at a different location, which is not correlated to the location of the first scattering event. This MS-related initial decay of the correlation function is typically described as an exponential-with the decay constant being proportional to the amount of scattering events per photon path [11]. By contrast, a purely diffusive decay of this function is on the order of ms and slower, depending on the strength of the interaction and the investigated scattering vector [44]. This time scale separation applies to both homodyne and heterodyne scattering.

Since the decays in time domain originate from different, statistically uncorrelated processes, their Fourier transforms are also statistically independent and simply super-impose. Further, the pronounced difference in time scales translates into a pronounced difference in the width of the corresponding super-imposed Lorentzians (c.f. Fig. 8). Then our empirical scheme is able to separate both spectral contributions via suitable fits. In the field free case the Lorentzians are both centred at the frequency of the Bragg-shift of 2 kHz corresponding to an average drift velocity of zero.

In the present study correction scheme was applied in several cases. It was utilized to i) quantify the drift motion in an electric field, ii) investigate the still incompletely understood spectral broadening under flow, and iii) different types of Brownian motion. For PnBAPS118, the self-diffusion coefficient was observed to decrease to a saturation value. However, the more dilute sample showed the slower temporal evolution. We believe, that this observations contain interesting information about the disappearance of grain boundary volume with time and thus in future experiments complement existing structural studies on coarsening samples [57, 58, 59, 60]. For these, it seems of particular importance, that depending on the optical properties of the chosen particles, one may study either self- or collective diffusion. Further, one may exploit the possibility of q -dependent measurements down to very small q values that are out of reach for most commercial DLS set-ups. At dominant coherent scattering, the hydrodynamic function can be measured, while for suspensions of similar interactions, but strong optical polydispersity, the corresponding self-dynamics will become accessible. At larger angles the dynamic structure factor can be measured. In particular for non-ergodic samples like polycrystalline or glassy suspensions, it may turn out to be very useful to directly measure $g_E(q,t)$ instead of $g_I(q,t)$ [61]. However, quantification of stretched exponential

relaxation processes may be cumbersome in frequency domain. We therefore anticipate that our approach to MS-corrected heterodyne light scattering will turn out very versatile and useful far beyond velocity measurements.

We finally shortly comment on our electro-kinetic results. We found that μ_e first increases, then it displays a more or less pronounced plateau and finally it decreases again. We believe that this indicates a universal behaviour and reconciles previously made mutually incompatible observations on the density dependence of the electro-phoretic mobility. These data were gathered for particles of different surface chemistry and size, at fully deionized conditions and in the presence of salt, each covering different parts of the universal curve.

However, we also observe a significant scatter in our data. All our measurements were performed after contact with an ambient air. Possibly, the limiting value for the electrolyte content was not reached in all situations. Therefore, the observed scatter in the measured mobilities may reflect the salt concentration dependence of the mobility. This limits our present analysis to the qualitative demonstration of the existence of a maximum in μ_e and excludes any further interpretation of the observed electro-kinetic mobilities. Additional measurements, utilizing particles of different surface chemistry as well as the conditioning set-up to precisely control the electrolyte content, are currently under way.

Conclusion

We have introduced a simple yet powerful empirical correction scheme for super-heterodyne light scattering in frequency domain. We demonstrated its scope and limits by systematic LDV measurements on charged particles subjected to an electric field and by the frequency domain complements of diffusion measurements on weakly and strongly interacting suspensions. We discussed its versatility and limits and indicated a variety of possible applications beyond electro-kinetics. We anticipate that this approach will allow for a number of interesting investigations on the dynamic properties of turbid suspensions at moderate to very low transmittance.

Acknowledgements

We gratefully acknowledge many fruitful and in the best sense, controversial discussions with our theoretical colleagues G. Nägele, A. Delgado, F. Carrique, E. Ruiz-Reina, R. Roa, V. Lobaskin, B. Dünweg, and C. Holm who strongly motivated the improvements made. We thank S. Heidt and S. Sreij for the PI-determination of PnBAPS118. Financial support of the DFG (SPP 1726 and Pa459/19) as well as of Interne Forschungsförderung, JGU is gratefully

acknowledged. L.M.M. further gratefully acknowledges financial support by the DAAD IAESTE program.

References

- [1] P. N. Pusey, *Curr. Opin. Colloid Interface Sci.* **4**, 177-185 (1999). Suppression of multiple scattering by photon cross-correlation techniques
- [2] G. Maret, *Curr. Opinion Colloid Interface Sci.* **2**, 251-257 (1997). Diffusing Wave Spectroscopy
- [3] A. Vrij, J. W. Jansen, J. K. G. Dhont, C. Pathmamanoharan, M. M. Kopswekhoven, H. M. Fijnaut, *Faraday Discuss* **76**, 19-35 (1983). Light-scattering of colloidal dispersions in non-polar solvents at finite concentrations - silica spheres as model particles for hard-sphere interactions.
- [4] W. van Megen, T. C. Mortensen, S. R. Williams, J. Müller, *Phys. Rev. E* **58**, 6073-6085 (1998). Measurements of the self-intermediate scattering function of suspensions of hard spherical particles near the glass transition
- [5] K. Okoshi, N. Sano, T. Okumura, A. Tagaya, J. Magoshi, Y. Koike, M. Fujiki, J. Watanabe, *J. Colloid Interface Sci.* **263**, 473-477 (2003). The Christiansen effect of brightly colored colloidal dispersion with an amphiphilic polymer
- [6] F. Stieber, W. Richtering *Langmuir* **11**, 4724-4727 (1995). Fiber-Optic-Dynamic-Light-Scattering and Two-Color-Cross-Correlation Studies of Turbid, Concentrated, Sterically Stabilized Polystyrene Latex
- [7] G. D. J. Phillies, *Phys Rev A* **24**, 1939-1943 (1981). Experimental demonstration of multiple-scattering suppression in quasielastic-light-scattering spectroscopy by homodyne coincidence techniques.
- [8] K. Schätzel, *J. Modern Optics* **38**, 1849-1865 (1991). Suppression of Multiple Scattering by Photon Cross-Correlation Techniques
- [9] B. J. Berne and R. Pecora, *Dynamic light scattering*, John Wiley, New York, 1976
- [10] T. Araki, H. Tanaka, *EPL* **82**, 18004 (2008). Physical principle for optimizing electrophoretic separation of charged particles

-
- [11] D. Pine, Light scattering and rheology of complex fluids far from equilibrium, in: M. Cates and M. Evans, eds., *Soft and Fragile Matter: Nonequilibrium Dynamics, Metastability and Flow*, J. W. Arrowsmith Ltd, Bristol, 2000
- [12] S. Takagi and H. Tanaka, *Phys. Rev. E* **81**, 021401 (2010). Multiple-scattering-free light scattering spectroscopy with mode selectivity
- [13] A. Delgado, F. González-Caballero, R.J. Hunter, L.K. Koopal, J. Lyklema, *J. Colloid Interface Sci.* 309, 194–224 (2007). Measurement and interpretation of electro-kinetic phenomena
- [14] J. D. Posner, *Mechanics Research Communications* 36 22–32 (2009). Properties and electro-kinetic behavior of non-dilute colloidal suspensions
- [15] D. E. Dunstan, L. A. Rosen, D. A. Saville, *J. Colloid Interface Sci.* 153, 581-583 (1992). Particle Concentration Effects on the Electrophoretic Mobility of Latex Particles
- [16] T. Bellini, V. Degiorgio, F. Mantegazza, F.A. Marsan, C. Scarnecchia, *J. Chem. Phys.* 103, 8228 (1995). Electro-kinetic properties of colloids with variable charge: I electrophoretic and electrooptic characterization.
- [17] M. Evers, N. Garbow, D. Hessinger, T. Palberg, *Phys. Rev. E* 57, 6774 - 6784 (1998). Electrophoretic mobility of interacting colloidal spheres
- [18] T. Palberg, M. Medebach, N. Garbow, M. Evers, A. Barreira Fontecha, H. Reiber, *J. Phys. Condens. Matter* 16, S4039 - S4050 (2004). Electro-phoresis of model colloidal spheres in low salt aqueous suspension
- [19] M. Medebach, T. Palberg, *J. Phys. Condens. Matter* 16, 5653 - 5658 (2004). Electrophoretic mobility of electrostatically interacting colloidal spheres
- [20] V. Lobashkin, B. Dünweg, C. Holm, M. Medebach, T. Palberg, *Phys. Rev. Lett.* 98, 176105 (1-4) (2007). Electro-phoresis of colloidal dispersions in counterion-dominated screening regime
- [21] T. Palberg, H. Schweinfurth, T. Köller, H. Müller, H. J. Schöpe, A. Reinmüller, *Eur. Phys. J. Special Topics* **222**, 2835-2853 (2013). Structure and transport properties of charged sphere suspensions in (local) electric fields
- [22] F. Carrique, E. Ruiz-Reina, R. Roa, F. J. Arroyo, Á. V. Delgado, *J. Colloid Interface Sci.* 455 46-54 (2015). General electro-kinetic model for concentrated suspensions in aqueous

electrolyte solutions: Electrophoretic mobility and electrical conductivity in static electric fields

[23] M. Medebach, T. Palberg, *Colloid Surf. A* **222**, 175 – 183 (2003).
Colloidal crystal motion in Electric Fields

[24] T. Palberg, H. Versmold, *J. Phys. Chem.* **93**, 5296-5310 (1989).
Electrophoretic-electroosmotic light scattering

[25] J. F. Miller, K. Schätzel, and B. Vincent, *J. Colloid Interface Sci.* **143**, 532–554, (1991). The determination of very small electrophoretic mobilities in polar and nonpolar colloidal dispersions using phase analysis light scattering

[26] K. Schätzel, W. Weise, A. Sobotta, M. Drewel, *J. Colloid Interface Sci.* **143**, 287-293 (1991). Electro-osmosis in an Oscillating Field: Avoiding Distortions in Measured Electrophoretic Mobilities

[27] T. Palberg, T. Köller, B. Sieber, H. Schweinfurth, H. Reiber, and G. Nägele. *J. Phys.: Condens. Matter* **24**, 464109 (2012). Electro-kinetics of Charged-Sphere Suspensions Explored by Integral Low-Angle Super-Heterodyne Laser Doppler Velocimetry

[28] T. Palberg, H. Versmold, *J. Phys. Chem.* **93**, 5296-5310 (1989). Electrophoretic-electroosmotic light scattering

[29] J.F. Miller, *J. Colloid Interface Sci.* **153**, 266 (1992). Electrophoretic light scattering using sinusoidal electric fields

[30] J. F. Miller, K. Schätzel, B. Vincent, *J. Colloid Interface Sci.* **143**, 532 (1991). The determination of very small electrophoretic mobilities in polar and nonpolar colloidal dispersions using phase analysis light scattering

[31] J. K.G. Dhont, C. G. De Kruif, A. Vrij, *J. Colloid Interface Sci.* **105**, 539-555. Light scattering in colloidal dispersions: Effects of multiple scattering

[32] J. K. G. Dhont, *An introduction to the dynamics of colloids*, Elsevier, Amsterdam 1996.

[33] B. R. Ware, *Adv. Coll. Interface Sci.* **4**, 1 (1974).

[34] G. I. Taylor, *Proc. Roy. Soc. London A* **219**, 186 (1954) and **223**, 446 (1954).

[35] G. Nägele, et al. private communication

-
- [36] P. White, *Phil. Mag.* **23**, 811-823 (1937). The theory of electroosmotic circulation in closed vessels
- [37] S. Komagata, *Researches Electrotech. Lab. Tokyo Comm.* **348**, 1-114 (1933).
- [38] J. K. G. Dhont and W. J. Briels, *Rheol Acta* **47**, 257–281 (2008). Gradient and Vorticity Banding
- [39] T. Palberg, M. Würth, *J. Phys I (France)* **6**, 237-244 (1996). Multiphase coexistence and non-linear rheology of colloidal suspensions in an optical model capillary viscosimeter
- [40] M. Medebach, T. Palberg, *J. Chem. Phys.* **119**, 3360 – 3370 (2003). Phenomenology of Colloidal Crystal Electro-phoresis
- [41] M. Medebach, L. Shapran, T. Palberg, *Colloid Surfaces B* **56**, 210 – 219 (2007). Electrophoretic flow behaviour and mobility of colloidal fluids and crystals
- [42] M. Medebach, T. Palberg, *Colloid Surf. A* **222**, 175 – 183 (2003). Colloidal crystal motion in Electric Fields
- [43] W. Härtl, H. Versmold, *J. Chem. Phys.* **80**, 1387 (1984). An experimental verification of incoherent light scattering
- [44] G. Nägele, *Phys. Reports* **272**, 217 (1996). On the dynamics and structure of charge-stabilized suspensions
- [45] M. Medebach, *J. Chem. Phys.* **136**, 044201 (2012). Influence of structure in heterodyne electrophoretic light scattering.
- [46] M. Watzlawek and G. Nägele, *Phys. Rev. E* **56**, 1258 (1997). Self-Diffusion Coefficients of Charged Particles: Prediction of Non-linear Volume Fraction Dependence
- [47] A. G. Mailer, P. S. Clegg and P. N. Pusey, *J. Phys.: Condens. Matter* **27** 145102 (2015). Particle sizing by dynamic light scattering: non-linear cumulant analysis
- [48] T. Palberg, W. Härtl, U. Wittig, H. Versmold, M. Würth, E. Simnacher, *J. Phys. Chem.* **96**, 8180-8183 (1992). Continuous deionization of latex suspensions
- [49] D. Hessinger, M. Evers, T. Palberg, *Phys. Rev. E* **61**, 5493 - 5506 (2000). Independent Ion Migration in Suspensions of Strongly Interacting Charged Colloidal Spheres

-
- [50] P. Wette, H.-J. Schöpe, R. Biehl, T. Palberg, *J. Chem. Phys.* **114**, 7556 - 7562 (2001). Conductivity of deionised two-component colloidal suspensions
- [51] H.-J. Schöpe, T. Palberg: *J. Colloid Interface Sci.* **233**, 149-161 (2001). A multipurpose instrument to measure the vitreous properties of charged colloidal solids
- [52] P. Wette, H.-J. Schöpe T. Palberg, *Colloid Surf. A* **222**, 311 – 321 (2003). Experimental Determination of Effective Charges in Aqueous Suspensions of Colloidal Spheres
- [53] L. Shapran, M. Medebach, P. Wette, H. J. Schöpe, T. Palberg, J. Horbach, T. Kreer, A. Chatterji, *Colloid. Surf. A* **270**, 220-225 (2005). Qualitative characterisation of effective interactions of charged spheres on different levels of organisation using Alexander's renormalised charge as reference
- [54] R. J. Spry, D. J. Kosan, *Appl. Spectroscopy* **40**, 782-784 (1986). Theoretical Analysis of the Crystalline Colloidal Array Filter
- [55] F. Bitzer, T. Palberg, H. Löwen, R. Simon, P. Leiderer, *Phys. Rev. E* **50**, 2821-2826 (1994). Dynamical test of interaction potentials for colloidal suspensions
- [56] D. G. Grier, C. A. Murray, *J. Chem. Phys* **100**, 9088 (1994). The microscopic dynamics of freezing in supercooled colloidal fluids.
- [57] A. Stipp, T. Palberg, E. Bartsch, *Phys. Rev. Lett.* **102**, 038302 (2009). Unusual crystallization kinetics in a hard sphere colloid - polymer mixture
- [58] A. Stipp, H. J. Schöpe, T. Palberg, T. Eckert, R. Biehl, E. Bartsch, *Phys. Rev. E* **81**, 051401 (2010). Optical experiments on a crystallization hard sphere - polymer mixture at coexistence
- [59] M. Shinohara, A. Toyotama, M. Suzuki, Y. Sugao, T. Okuzono, F. Uchida, and J. Yamanaka, *Langmuir* **29**, 9668–9676 (2013). Recrystallization and Zone Melting of Charged Colloids by Thermally Induced Crystallization
- [60] N. Ghofraniha, E. Tamborini, J. Oberdisse, L. Cipelletti, and L. Ramos, *Soft Matter* **8**, 6214-6219 (2012). Grain refinement and partitioning of impurities in the grain boundaries of a colloidal polycrystal
- [61] W. van Meegen, S. M. Underwood, and P. N. Pusey, *Phys. Rev. Lett.* **67**, 1586-1589 (1991). Nonergodicity parameters of colloidal glasses